The Journal of Experimental Biology 206, 255-267

doi:10.1242/jeb.00078

Copepod feeding currents: flow patterns, filtration rates and energetics

Luca A. van Duren*, Eize J. Stamhuis and John J. Videler

Department of Marine Zoology, University of Groningen, PO Box 14, 9750 AA Haren, The Netherlands

*Author for correspondence at present address: NIOO-CEME/KNAW, PO Box 140, 4400 AC, Yerseke, The Netherlands (e-mail: duren@cemo.nioo.knaw.nl)

Accepted 14 October 2002

Summary

Particle image velocimetry was used to construct a quasi 3-dimensional image of the flow generated by the feeding appendages of the calanoid copepod *Temora longicornis*. By scanning layers of flow, detailed information was obtained on flow velocity and velocity gradients.

The flow around feeding *T. longicornis* was laminar, and was symmetrical viewed dorsally, but highly asymmetrical viewed laterally, with high levels of vorticity on the ventral side. The flow rate through the feeding appendages varied between 77 and 220 ml day^{-1} per individual. The morphology of the flow field ensured that water was entrained over the full length of the first antennae. These were kept out of areas with high velocity gradients that could interfere with distant mechano- or chemoreception.

The volume of influence, i.e. the volume of water around the foraging copepod, where shear rates were significantly higher than background levels, was calculated. Implications for encounter probability and mechanoreception are discussed. The average rate of energy dissipation within the copepod's volume of influence is several times higher than the levels of turbulent energy dissipation these animals are likely to encounter in their environment. Even in highly turbulent environments, adult *T. longicornis* will not experience very significant effects of turbulence.

Within the volume of influence of the copepods the energy dissipation due to viscous friction varied between 6.6×10^{-11} and 2.3×10^{-10} W. Taking mechanical efficiency and muscle efficiency into account, this results in a total energetic cost of the feeding current of 1.6×10^{-9} W per copepod. This value represents only a small percentage of the total energy budget of small calanoid copepods.

Key words: copepod, *Temora longicornis*, feeding current, hydrodynamics, energetics.

Introduction

Temora longicornis (Müller) is a small calanoid copepod, very abundant in the North Sea. Calanoid copepods commonly use the mouth appendages to create a feeding current, which is scanned for food items (Strickler, 1985; Alcaraz et al., 1980). The feeding current propels the animals forward and draws food towards the mouth appendages.

The copepodid stages of *T. longicornis* show a smooth swimming motion with very few jumps or hops (van Duren and Videler, 1995). Average swimming speeds range from <2 to >12 mm s^{-1} for adult animals. The feeding appendages move nearly 100% of the time. *T. longicornis* creates its feeding current with a coordinated movement of all the cephalic appendages with the exception of the first antennae. The second antennae are most important in generating propulsive thrust but the mandibular palps and the first maxillae contribute to the backward movement of water as well.

The strength of the feeding current directly relates to the feeding rate. The current also plays an important role in providing the copepod with information about its environment and it transfers signals from the copepod to organisms in its vicinity.

Another important aspect is the energetic cost involved in creating velocity gradients in the water. For copepods, assessing the cost of moving in water has proved to be a difficult task (Vlymen, 1970; Klyashtorin and Yarzhombek, 1973; Morris et al., 1985, 1990). Cost of swimming estimates are mostly based on models and range from 0.3% to 30–40% of the total energy budget.

With the recent developments in imaging technology it has become possible to visualise and investigate flow around small organisms quantitatively (Yen et al., 1991; Fields and Yen, 1993; Strickler, 1985; Bundy and Paffenhöfer, 1996; Stamhuis and Videler, 1995). Quantitative data on flow can be used to calculate the viscous dissipation of energy into the water (Yen et al., 1991). The results of the calculations serve as a basis on which to estimate the total cost of the feeding current.

This study will apply laser sheet particle image velocimetry (PIV) (Stamhuis and Videler, 1995) to analyse the flow of the feeding current of adult female *T. longicornis* and to construct a quasi 3-D impression of the velocity gradients in the water. The volume of water flowing over the feeding appendages will

Table 1. *Animal statistics and experimental details*

Animal	Length (mm)	AFDM (μg)*	Animal volume (mm^3)**	View	Number of planes	Number of data points
t6l	0.72	11.457	0.0426	Dorsal	7	3520
t5f	0.77	14.074	0.0479	Dorsal	9	3619
t5f	0.77	14.074	0.0479	Lateral	9	3743
t5b	0.81	16.436	0.0570	Dorsal	8	2951
t5b	0.81	16.436	0.0570	Lateral	7	2225
t5d	0.81	16.436	0.0609	Lateral	9	4879
t5a	0.94	25.933	0.0972	Dorsal	8	3908
t5k	1.01	32.317	0.1166	Dorsal	11	6445
t5k	1.01	32.317	0.1166	Lateral	14	9158

AFDM, ash-free dry mass.

*Calculated after Klein Breteler et al. (1982).

**Calculated using length, width and depth measurements and assuming the body shape to be an eliptoid.

be estimated and compared to available data of filtering rates. From the velocity, the volume of influence (i.e. the volume of water where the animal has a significant influence on the water) is calculated. Increase in encounter probability is assessed and possible effects of environmental turbulence on feeding rates are discussed. Subsequently, the collected data are used to estimate the rate of energy dissipation due to viscous friction, and an estimate is made of the total energetic cost of the feeding current and its impact on the overall energy budget of this copepod species.

Materials and methods

Experimental animals

Temora longicornis Müller were cultured in the laboratory, where they were fed on a mixture of algae (*Rhodomonas* sp. and *Isochrysis galbana*) from continuous cultures. In the copepod culture the heterotrophic flagellate *Oxyrrhis marina* was present as an additional food source (Klein Breteler and Gonzales, 1986). The temperature of the culture was maintained at 15°C.

Table 1 gives the details of the experimental animals used. Ash-free dry masses (AFDM) were calculated using the length–mass relationship from Klein Breteler et al. (1982).

Tethering

During the experiments the animals were tethered by a suction restraint method, similar to the technique described by Gill (1987). Instead of using polythene tubing the animals were attached to a thinly drawn glass pipette. The tip of the pipette was hand polished until completely smooth to avoid damaging the animals and to create a tight seal between the carapace and the tip of the pipette.

The copepods were anaesthetized in a 0.02% solution of MS-222 (Sandoz) and carefully transferred to the experimental vessel. The dorsal side of the carapace of the anaesthetized animals was gently sucked against the tip of the pipette. The animals were manoeuvred in the desired position and subsequently allowed to recover for at least 15 min. The tethering did not restrict the animals in their limb movements. Once the underpressure in the pipette was released after experiments the animals were observed to swim away unharmed.

Particle image velocimetry

Laser sheet particle image velocimetry (PIV) involves recording the displacement of particles representing the flow of water in one plane illuminated by a thin sheet of laser light. From the displacement of the particles over time, velocity vectors are derived, and these in turn can be used to study characteristics of the flow such as spatial distribution of velocity, spatial acceleration, vorticity, strain and shear. The technique comprises three stages: image acquisition, image analysis and flow field analysis. For details, see Stamhuis and Videler (1995).

Image acquisition

Recording equipment

A perspex experimental vessel (dimensions: 6 cm×6 cm×4 cm) was filled with seawater and seeded with nylon beads (TSI Inc., diameter 4±1.2 μm, ± S.D.). These particles were illuminated in one plane using a horizontally positioned, 0.2 μm thick laser light sheet (Fig. 1) from a red light Krypton laser (Coherent Innova 70K, λ=647 nm, P_{max}=1 W). A black and white CCD video camera (I2s: IEC862BC, resolution 768×512 pixels) was mounted above the vessel, perpendicular to the light sheet. The camera was fitted with a 17–68 mm zoom lens (Angénieux) and a 70 mm extension ring, resulting in a total field of view of 5.30×3.74 mm. Movement of the particles was recorded on video tape (Sony U-matic SP) at 25 frames s^{-1}. Separate fields of frames were used for analysis to prevent video interlace blurring and to increase the maximum time resolution to 50 fields s^{-1}. This frequency is not enough to resolve the limb beat frequency of the copepods, which ranges between 20 and 50 Hz, depending on temperature, food and other factors.

Experimental procedure

The pipette with the tethered animal was mounted on a micromanipulator for precise positioning. At the start of each trial the animal was positioned in the light sheet with either the dorsal or the lateral side to the camera. It was left in this position for 1 min to avoid any effects on the flow from the positioning of the animal. To avoid any wall effects the light sheet was always at least 8 mm away from the bottom and the walls of the vessel and from the water surface. The feeding current of the copepod was filmed for 15 s to up to 1 min. Subsequently, the animal was repositioned with the micromanipulator 0.25 mm above the original position, and left for 1 min before the feeding current was filmed in the new position. This procedure was repeated with the animal 0.50, 0.75 mm, etc, above the light sheet until no effect from the animal on the water flow could be observed. The animal was

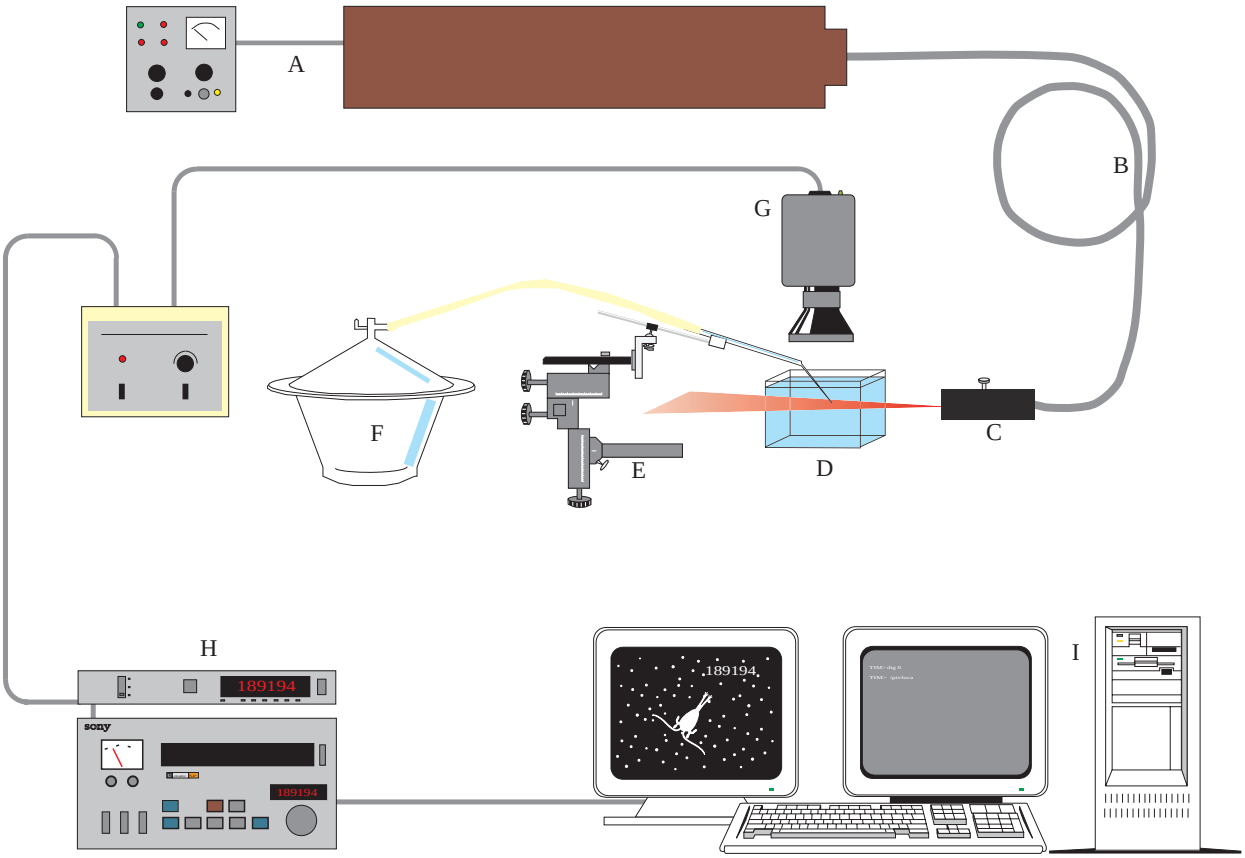

Fig. 1. Schematic drawing of the image acquisition setup. A, Krypton laser; B, optical fibre; C, optical probe; D, experimental vessel with seeded seawater and laser light sheet; E, micromanipulator with mounted pipette; F, desiccator; G, high-resolution video camera; H, video recorder; I, computerized image analysis system.

then placed back in the laser sheet and filmed again. Subsequently the same procedure was carried out with the animal positioned underneath the laser sheet with the last sequence filmed with the animal in the laser sheet again.

The flow was assumed to be constant over the amount of time one animal was filmed, so the different layers could be combined afterwards to construct a 3-D impression of the flow. To check whether the behaviour of the animal, and hence the flow field, changed over time, the different sequences of the animal in the laser sheet were compared, but significant changes were never observed over the course of time that an experiment took place.

Series of sequences of six adult female *T. longicornis* were filmed. From three of these both dorsal and lateral views were obtained, from two animals only a dorsal view and from one animal only a lateral view. The sizes of animals differed considerably and the number of planes filmed per series varied from 7 to 14 (Table 1). After each experiment the animals were anaesthetised again and length, width, depth of the body were measured and the length and span of the antennae and the length of the maxillipeds and maxillae.

Image analysis

We used two techniques to analyse the video recordings of feeding currents of adult females: particle tracking velocimetry (PTV) and a combination of sub-image correlation PIV (SCPIV) and PTV.

The PTV technique entails locating the position of individual particles in two subsequent video frames. Two images are binarized by a threshold operation, the particles in the two images are given separate colours, and then the images are superimposed. A cursor box is placed manually around two corresponding particles and the position of the particle in the two images was detected automatically. This technique works well with low seeding densities, but it is laborious and does not work as well in turbulent and hence unpredictable flow regimes.

SCPIV is not based on recognising individual particle pairs, but on the recognition of particle patterns in corresponding subimages. A cross-correlation is performed between pairs of subimages in two subsequent frames from the same location in each frame. The result of this routine is a peak with an offset from the sub-image centre corresponding to the average displacement of the particles between the two frames. This procedure is repeated with the next pair of subimages with an overlap of 50% until the whole frame has been scanned.

SCPIV has the advantage over PTV that it is fully automatic. It cannot, however, be used in areas very close to the surface of an animal and in areas with very high velocity gradients, in

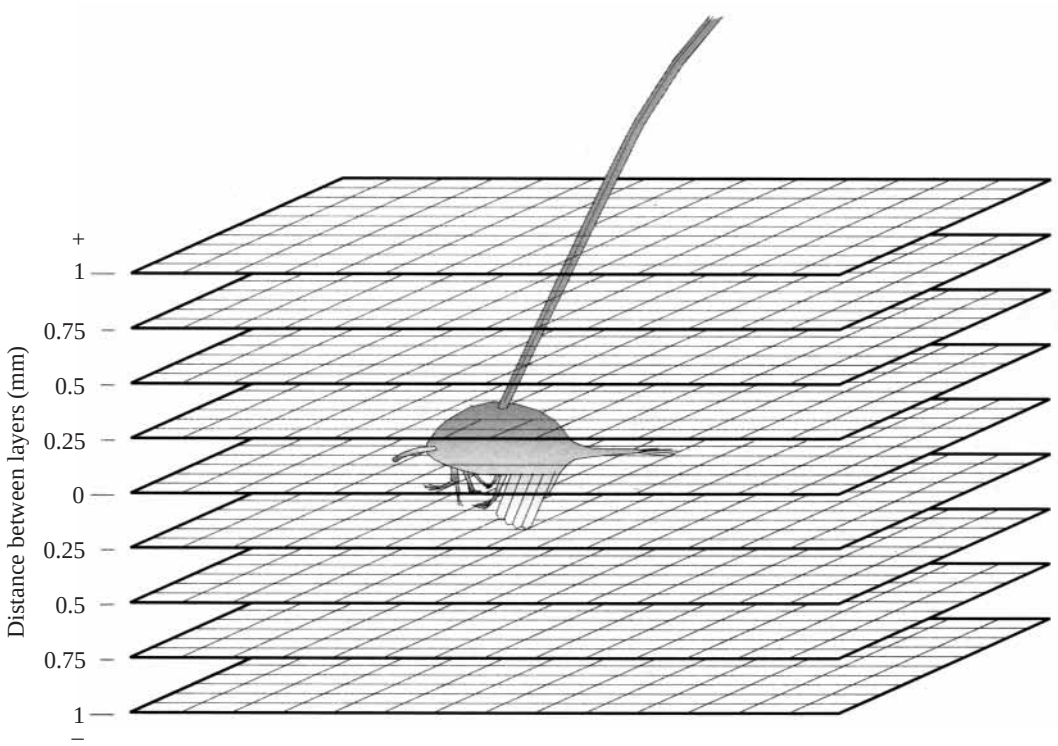

Fig. 2. Schematic drawing of construction of quasi-3D image of flow.

general also close to the moving appendages of the animal. We therefore combined the SCPIV and PTV technique by analysing the area close to the copepod with PTV and using the same two images to analyse the flow further away from the animal with SCPIV. The files from both analysis were subsequently combined and resulted in one flow field.

Although the maximum time resolution with this setup is 50 fields s^{-1}, one field was skipped between subsequent fields, to ensure sufficient displacement of particles between two fields. The tape speed is not sufficient to record the oscillations in the flow due to the beat frequency of the feeding appendages.

Flow field analysis

The processing involves the application of a grid, superimposed on the fields of view (Stamhuis and Videler, 1995). The resolution of the grid is adjusted to the number of available measured vectors from the combined SCPIV and PTV analysis, and grid resolution was the same for all the flow fields of one series of layers. Each cell of the grid is checked for the presence of vectors. Angle and magnitude of the vectors within a cell are averaged and 1 cell vector is placed at the centre of the cell. If a cell contains only 1 vector then that one becomes the cell vector.

A data validation is carried out to remove erroneous vectors that may have been introduced by misidentification of particle pairs during PTV procedures or errors occurring due to low local seeding density or occasional aggregates of particles during SCPIV routines. This data validation is based on the comparison of a vector with its neighbours, and takes into account the local variance and the variance of all the vectors in the flow field.

Remaining empty cells, situated inbetween cells containing a cell vector, are then filled using an iterative interpolation. No interpolation takes place across objects (e.g. the body or extremities of an animal) and no extrapolation is carried out. The result is a flow field with uniformly distributed vectors, from which gradient parameters such as vorticity (i.e. rate of change of direction of the fluid), shear rate (rate of change of velocity perpendicular to the direction of the flow) and acceleration rates can be calculated and displayed in colour-coded plots. For descriptive purposes, average flow or background flow can be subtracted from the vectors in the flow field. The centres of vortices can be accurately assessed by calculating the discriminant of complex eigenvalues (d) (Stamhuis and Videler, 1995). The area where the d has the largest negative value indicates the centre of a vortex system.

Post-processing

Calculating maximum filtration rates

From the lateral views on the videotape the maximum extension of the antennae, maxillae and the maxillipeds were estimated, and from the dorsal views the extent of the antennae in this plane was also measured (for all animals some dorsal and lateral views were available on tape, although for some individuals these images could not be included in the analysis). For each animal the following surface areas were calculated: the maximum cross section covered by the antennae (s-A2), by calculating the surface of a semi-ellipsoid based on the maximum extension of the antennae in the dorsal and lateral plane, and the maximum cross section covered by the maxillae (s-m2) and by the maxillipeds (s-mx), by calculating the surface of a semi-ellipsoid based on the width of the body and

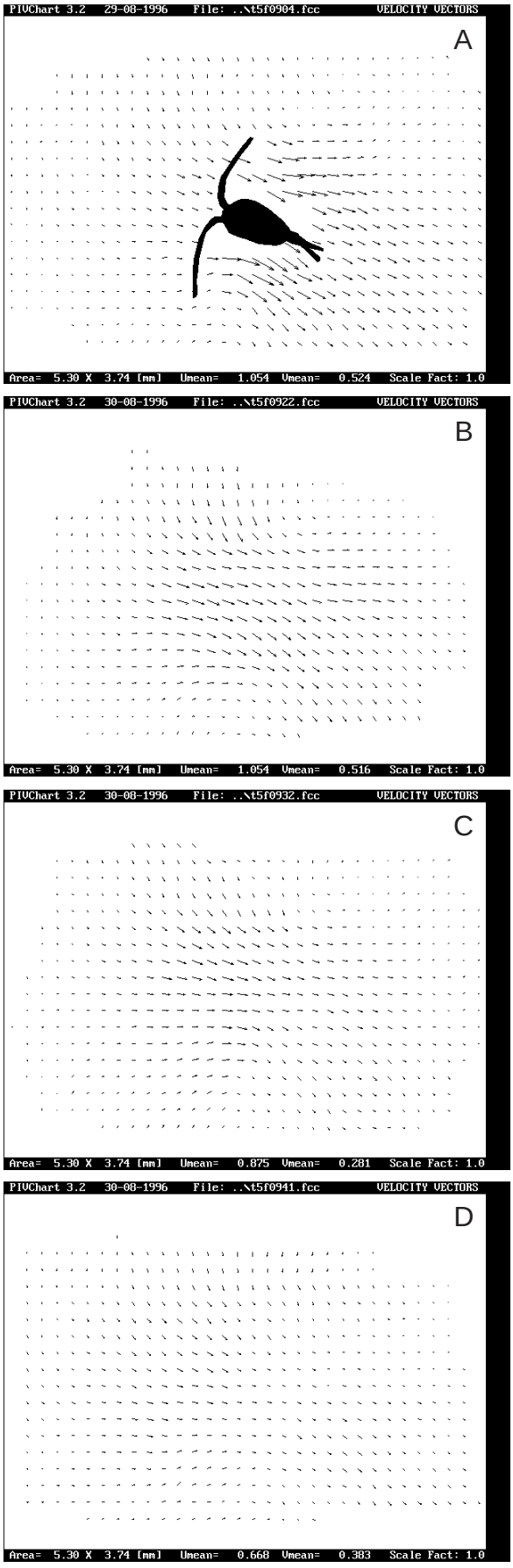

Fig. 3. Velocity vector diagram of the flow around a foraging copepod. Dorsal view (*XY* plane). (A) Animal in plane of focus, (B) plane of focus 0.25 mm to the ventral side of the copepod, (C) plane of focus 0.50 mm to the ventral side of the copepod, (D) plane of focus 0.75 mm to the ventral side of the copepod.

the extension of the maxillae and the maxillipeds, respectively. The surface areas were multiplied by the flow velocities measured around the appendages, yielding a volume of water flowing through the capture area.

Estimating the volume of influence

Due to the incompressible nature of water, the volume of water affected by the movements of an animal is theoretically infinite, but obviously velocity gradients decline asymptotically to background levels. In water without an animal present we still measure shear rates of up to $0.5\,s^{-1}$, due to background flow and slight digitising errors in the system. Yen and Fields (1992) found that *Acartia tonsa* nauplii showed escape reactions in the vicinity of foraging *T. longicornis* when shear rates in the flow field exceeded values of $0.8\,s^{-1.}$ We therefore defined the volume of influence around a copepod as the volume around the animal where the shear rate was $>0.7\,s^{-1}$.

To calculate this volume of influence, all the layers of an animal that were filmed, in either dorsal or lateral view, were combined. Cells in this 3-D grid had a surface area equal to the surface area of a cell in the flow field grid and a depth of 0.25 mm (the distance between the layers, Fig. 2). Total volume of influence was calculated as the sum total of the volumes of the grid cells where the shear threshold value was exceeded.

Calculating the rate of energy dissipation

A system of *x*, *y* and *z* Cartesian coordinates was defined around the copepod with velocity components **u**, **v** and **w** in the respective directions. The dorsal view on the copepod was considered to be the *XY*-plane, the lateral view the *XZ* plane and the anterior view was considered to be the *YZ* plane.

The rate of energy dissipation due to viscous friction (P) within a particular volume (V_i) can be calculated as:

$$P = \nu \sum V_i \Phi_i , \tag{1}$$

where P is expressed in W, ν is the dynamic viscosity, and Φ the dissipation function (Schlichting, 1979; Budó 1980):

$$\Phi = 2\left[\left(\frac{\partial \mathbf{u}}{\partial x}\right)^2 + \left(\frac{\partial \mathbf{v}}{\partial y}\right)^2 + \left(\frac{\partial \mathbf{w}}{\partial z}\right)^2\right] + \left(\frac{\partial \mathbf{u}}{\partial y} + \frac{\partial \mathbf{v}}{\partial x}\right)^2 + \left(\frac{\partial \mathbf{u}}{\partial z} + \frac{\partial \mathbf{w}}{\partial x}\right)^2 + \left(\frac{\partial \mathbf{v}}{\partial z} + \frac{\partial \mathbf{w}}{\partial y}\right)^2 - \frac{2}{3}\left(\frac{\partial \mathbf{u}}{\partial x} + \frac{\partial \mathbf{v}}{\partial y} + \frac{\partial \mathbf{w}}{\partial z}\right)^2 . \tag{2}$$

In an incompressible fluid:

$$\frac{\partial \mathbf{u}}{\partial x}+\frac{\partial \mathbf{v}}{\partial y}+\frac{\partial \mathbf{w}}{\partial z}=0\,. \quad (3)$$

Therefore, the last component of Φ=0. Subsequently, Φ can be resolved into three factors, each factor representing one plane, so that

$$\Phi_{\mathrm{tot}}=\Phi_{\mathrm{XY}}+\Phi_{\mathrm{XZ}}+\Phi_{\mathrm{YZ}}\,, \quad (4)$$

where

$$\Phi_{\mathrm{XY}}=\left(\frac{\partial \mathbf{u}}{\partial x}\right)^2+\left(\frac{\partial \mathbf{v}}{\partial y}\right)^2+\left(\frac{\partial \mathbf{u}}{\partial y}+\frac{\partial \mathbf{v}}{\partial x}\right)^2, \quad (5)$$

$$\Phi_{\mathrm{XZ}}=\left(\frac{\partial \mathbf{u}}{\partial x}\right)^2+\left(\frac{\partial \mathbf{w}}{\partial z}\right)^2+\left(\frac{\partial \mathbf{u}}{\partial z}+\frac{\partial \mathbf{w}}{\partial x}\right)^2 \quad (6)$$

and

$$\Phi_{\mathrm{YZ}}=\left(\frac{\partial \mathbf{v}}{\partial y}\right)^2+\left(\frac{\partial \mathbf{w}}{\partial z}\right)^2+\left(\frac{\partial \mathbf{v}}{\partial z}+\frac{\partial \mathbf{w}}{\partial y}\right)^2. \quad (7)$$

The copepod moves water past its body from front to back. Consequently, particle motion in the anterior view (*YZ* plane) is very small compared to that in the lateral and the dorsal view. Applying the laser sheet filming technique in the *YZ* plane hardly provides useful information since virtually all the particle motion is directed at large angles to that plane. We assume therefore that the rate of energy dissipation shown by particles moving in this plane is negligibly small compared to that in the other two planes, and that:

$$P_{\mathrm{tot}}\approx P_{\mathrm{XY}}+P_{\mathrm{XZ}}\,. \quad (8)$$

For three adult females we have a full set of measurements in both the *XY* and *XZ* planes. For three other animals we have measurements in one plane, either dorsal or lateral. Although the intensity of the flow field may vary from animal to animal, it is not unreasonable to assume that the general shape of feeding currents of adult female copepods of one species does not vary much among individuals. Therefore the ratio of energy dissipation between the dorsal and lateral view will be similar. This ratio can then be used to estimate the energy dissipation rate for the animals for which we have only one set of measurements.

The average rate of energy dissipation per kg water within the volume of influence can be calculated by dividing the rate of energy dissipation by the volume of influence and the density of seawater.

Results

Flow morphology

T. longicornis shows a steady laminar flow along the body. The highest velocities and acceleration rates are measured around the tip of the feeding appendages. This means that the highest velocities occur not in the planes in which the body of the animal is situated, but in the *XY* plane just on the ventral side of the animal and in the *XZ* planes adjacent to the body. Fig. 3A–D shows the dorsal views of the flow fields in the plane around a copepod and of the parallel planes 0.25, 0.5 and 0.75 mm underneath the same animal. Fig. 4A–D shows the lateral views of the flow fields around the animal and at a distance of 0.25, 0.5 and 0.75 mm towards the camera from the animal. The maximum distance from the animal where a significant influence of the animal could still be measured on the water varied from 0.75 mm to 1.5 mm, in the case of a very large animal.

The flow is symmetrical along the body axis of the animal in the dorsal view, but the lateral views show a clear asymmetry with a large vortex system at the ventral side. This is illustrated in Fig. 5, where the vorticity field and the value of *d* (the discriminant of complex eigenvalues) in a series of parallel lateral flow fields is shown. The asymmetrical shape of the flow is obvious up to a distance of at least 0.75 mm from the centre of the body, coinciding with the distance within reach of the first antennae. Note that the colour coding is relative. The general shape of the vorticity field remains the same, but the values of maximum vorticity decrease in planes further away from the animal. The centre of the vortex does not change in position relative to the animal in the planes within reach of the first antennae (Fig. 5E–H). Beyond this point the centre shifts to the ventral side, becomes less defined and dissipates.

Potential filtration rates

Table 2 shows the estimates of flow through the area covered by the feeding appendages. Average values for the

Table 2. *Volumes of water passing through capture area*

Animal	Length (mm)	Surface (mm^2) A2	Surface (mm^2) mxp	Surface (mm^2) mx2	Velocity ($mm\ s^{-1}$)	VSC ($ml\ ind^{-1}\ day^{-1}$) A2	VSC ($ml\ ind^{-1}\ day^{-1}$) mxp	VSC ($ml\ ind^{-1}\ day^{-1}$) mx2
t6l	0.72	0.201	0.137	0.069	4.473	77.86	53.03	26.52
t5f	0.77	0.191	0.140	0.075	8.370	137.89	101.53	54.49
t5b	0.81	0.225	0.181	0.101	4.325	84.24	67.67	37.60
t5d	0.81	0.225	0.187	0.097	5.985	116.58	96.91	50.12
t5a	0.94	0.350	0.325	0.136	7.317	221.10	205.25	86.23
t5k	1.01	0.305	0.297	0.145	7.735	203.79	198.55	97.22

VSC, volume swept clear; ind, individual.

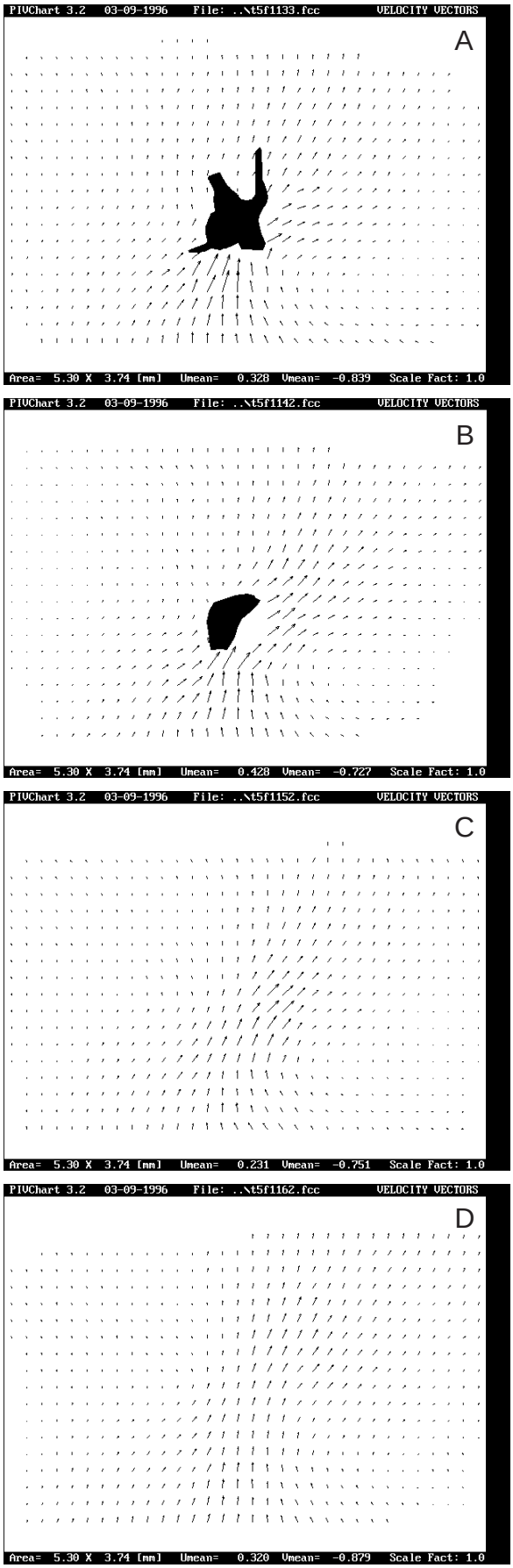

Fig. 4. Velocity vector diagram of the flow around a foraging copepod. Lateral view (*XZ* plane). (A) Animal in plane of focus, (B) plane of focus 0.25 mm to the lateral side of the copepod, (C) plane of focus 0.50 mm to the lateral side of the copepod, (D) plane of focus 0.75 mm to the lateral side of the copepod.

flow rate through the area covered by the antennae ranged around 140 ml individual^{-1} day^{-1}. Flow rate through the area swept by the maxillipeds (volume swept clear) ranged around 120 ml individual^{-1} day^{-1}, while through the area swept by the maxillae flow rates averaged just under 60 ml individual^{-1} day.

Velocity gradients and volume of influence

The dorsal view with the animal in the plane of focus shows that the highest shear rates occur around the area of the propulsive appendages (Fig. 6A). The area in front of the first antennae is remarkably calm. The lateral views show distinct maximums in the shear rate anterio-ventral of the animal (Fig. 6B–D). This maximum becomes less pronounced in more lateral planes beyond the tip of the antennae. The position of the first antennae is just outside this high shear area. In all the copepods analysed, the flow over the distal tips varied consistently between 1 mm s^{-1} and 1.5 mm s^{-1}.

Table 3 shows the volume of influence measured, the values of the parameters necessary to calculate the ranges of influence, the rate of energy dissipation and the mass-specific rate of energy dissipation. On average the copepods had a volume of influence of 12.52 mm^3, corresponding to a volume of water more than 180 times as large as their own body volume.

Energy dissipation

The measured volume of influence and the rates of energy dissipation were of the same order of magnitude in the dorsal and lateral measurements of the same animal (Table 3). The average ratio between energy dissipation in the dorsal and the lateral planes of the three individuals where both views were analysed was 0.9. This ratio was used to estimate the total energy dissipation in those individuals where only one plane was analysed. The rate at which energy dissipates increases with the volume of influence (Fig. 7). Larger animals tended to have larger ranges of influence (Fig. 8), although this relationship was not quite significant (P=0.08).

For three levels of ambient turbulence (10^{-3}, 10^{-2} and 10^{-1} cm^2 s^{-3}) we have calculated for each cell of each volume of influence whether the level of energy dissipation was higher or lower than the level of turbulent kinetic energy dissipation. If the level of energy dissipation in a cell was lower, the volume of this cell was subtracted from the volume of influence; if the level was higher, this cell was considered to be unaffected by ambient turbulence. Table 4 indicates for each animal which percentage of the volume of influence is unaffected at a particular level of turbulence. At a level of 10^{-3} cm^2 s^{-3}, none of the feeding currents would be affected; at 10^{-2} cm^2 s^{-3}, on average more than 80% of the feeding current still has a higher level of energy dissipation than the environment; at 10^{-1} cm^2 s^{-3}, less than 15% of the feeding current remains unaffected.

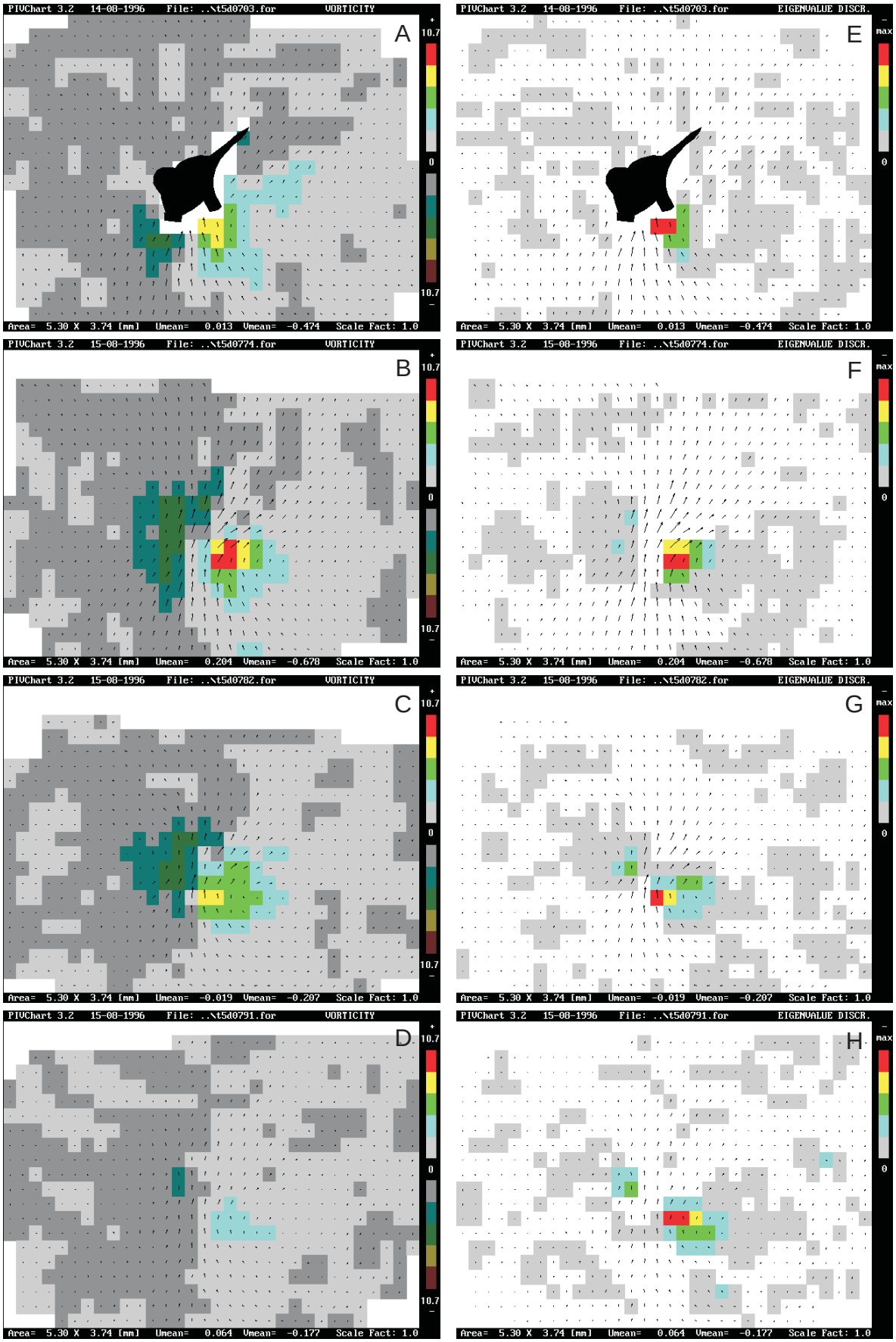
PIVChart 3.2 14-08-1996 File: ..\t5d0703.for VORTICITY
A
Area= 5.30 X 3.74 [mm] Umean= 0.013 Vmean= -0.474 Scale Fact: 1.0
PIVChart 3.2 14-08-1996 File: ..\t5d0703.for EIGENVALUE DISCR.
E
Area= 5.30 X 3.74 [mm] Umean= 0.013 Vmean= -0.474 Scale Fact: 1.0
PIVChart 3.2 15-08-1996 File: ..\t5d0774.for VORTICITY
B
Area= 5.30 X 3.74 [mm] Umean= 0.204 Vmean= -0.678 Scale Fact: 1.0
PIVChart 3.2 15-08-1996 File: ..\t5d0774.for EIGENVALUE DISCR.
F
Area= 5.30 X 3.74 [mm] Umean= 0.204 Vmean= -0.678 Scale Fact: 1.0
PIVChart 3.2 15-08-1996 File: ..\t5d0782.for VORTICITY
C
Area= 5.30 X 3.74 [mm] Umean= -0.019 Vmean= -0.207 Scale Fact: 1.0
PIVChart 3.2 15-08-1996 File: ..\t5d0782.for EIGENVALUE DISCR.
G
Area= 5.30 X 3.74 [mm] Umean= -0.019 Vmean= -0.207 Scale Fact: 1.0
PIVChart 3.2 15-08-1996 File: ..\t5d0791.for VORTICITY
D
Area= 5.30 X 3.74 [mm] Umean= 0.064 Vmean= -0.177 Scale Fact: 1.0
PIVChart 3.2 15-08-1996 File: ..\t5d0791.for EIGENVALUE DISCR.
H
Area= 5.30 X 3.74 [mm] Umean= 0.064 Vmean= -0.177 Scale Fact: 1.0

Fig. 5. Colour-coded plot of vorticity field (A–D) and the discriminant of complex eigenvalues *d* (E–H) around foraging copepod in parallel *XZ* planes. (A,E) Animal in plane of focus; (B,F) plane of focus 0.25 mm to the lateral side of the copepod; (C,G) plane of focus 0.50 mm to the side of the copepod; (D,H) plane of focus 0.75 mm to the side of the copepod.

Discussion

Method

Tethering

Although Hwang et al. (1993) found that tethering does not significantly alter the behaviour of copepods, there is no doubt that the morphology of flow fields will be to some extent different from those around moving animals. Instead of propelling itself through water, the animal has to accelerate water past itself. Tethering increases the volume of water moved by an animal (Emlet, 1990). Under normal food conditions *T. longicornis* moves relatively slowly, positioned vertically in the water column (Tiselius and Jonsson, 1990), so the influence of the tether on the morphology of the flow was probably limited.

The tether may have led to an overestimation of the volume of influence, but unless the animals changed their swimming effort as a result of the tether, the amount of dissipated energy in the water should remain the same.

The distance between the animal and the nearest wall was approximately 3 cm, and since the largest distance where any significant influence of the animal could be measured was 1.5 mm (in the case of a very large animal), wall effects in these experiments could safely be neglected.

Behaviour and feeding effort

Food concentration influences swimming speed (van Duren and Videler, 1995) and filtration rates (Lam and Frost, 1976) of copepods. Since no food was added to the water, the animals' feeding efforts may have been rather low. It is possible that presence of the nylon particles could have affected their feeding effort to some extent, but the size of these particles was at the lower end of the size range of normal dietary food particles (Poulet and Gill, 1988) and it is unlikely that the beads were perceived by the copepods, for example by mechanoreception (Légier-Visser et al., 1986).

Flow fields

Filtration rates

The velocity around the second antennae can be accurately assessed, but these extremities are not the main food-collecting appendages. What happens precisely inside the capture area cannot be observed with the present setup. The figures in Table 2 should therefore be treated as rough estimates.

Feeding rates are known to depend on the size of food. Berner (1962) reported 'volume swept clear' (VSC) values for adult female *T. longicornis* feeding on the small algae *Skeletonema costatum* (size 4–5 μm) between 0.5 and 13.5 ml copepod^{-1} day^{-1}. The feeding rate estimates in these experiments were based on tracer techniques, using the isotope ^{32}P, and compare quite well with the values we find for the volume of water passing over the second maxillae of the four smallest animals. Higher VSC values have been reported for *T. longicornis* feeding on other prey, with a maximum measurement of 95–245 ml copepod^{-1} day^{-1} (Paffenhöfer and Harris, 1976) when this species was feeding on the chain forming diatom *Thalassiosira rotula* (cell diameter 20–22 μm, chains up to 16 cells). This is fairly close to the values of flow through the maxillipeds we measured, particularly considering that feeding effort of the copepods was probably not very high due to the lack of available food. The increase of VSC with increasing food size could be due to increased retention efficiency of larger particles by the different feeding appendages involved in food capture, but it could also be a consequence of the fact that larger food particles may be detected earlier and, if necessary, redirected into the capture area. Paffenhöfer and Lewis (1990) found that the distance at which *Eucalanus pileatus* perceives *Thalassiosira weissflogii* cells increased twofold as food

Table 3. *Rate of energy dissipation due to viscous friction*

Animal	Length (mm)	Views	Range *XY* (mm^3)	Range *XZ* (mm^3)	Range tot** (mm^3)	Range:volume	P_{XY} (W)	P_{XZ} (W)	Ratio *XY*:*XZ*	P_{tot} (W)	P_{tot} g AFDM^{-1} (W g^{-1})
t6l	0.72	Dorsal	6.506	–	6.506	152.60	3.662×10^{-11}	–	0.9*	7.732×10^{-11}	6.748×10^{-6}
t5f	0.77	Both	12.615	13.528	13.528	282.21	7.458×10^{-11}	8.471×10^{-11}	0.9	1.593×10^{-10}	1.132×10^{-5}
t5b	0.81	Both	7.575	6.904	7.575	132.89	3.626×10^{-11}	2.926×10^{-11}	1.2	6.551×10^{-11}	3.986×10^{-6}
t5d	0.81	Lateral	–	11.988	11.988	196.98	–	5.093×10^{-11}	0.9*	9.676×10^{-11}	5.887×10^{-6}
t5a	0.94	Dorsal	9.815	–	9.815	101.01	6.543×10^{-11}	–	0.9*	1.381×10^{-10}	5.327×10^{-6}
t5k	1.01	Both	17.161	25.680	25.680	220.22	9.037×10^{-11}	1.647×10^{-10}	0.5	2.550×10^{-10}	7.892×10^{-6}
Mean	0.84				12.52	180.98				1.32×10^{-10}	6.86×10^{-6}
±S.E.M.	±0.05				±2.84	±26.81				$\pm2.86\times10^{-11}$	±1.04×10

*The value 0.9 is the average ratio of energy dissipation between the dorsal and lateral view of animals t5b, t5f, and t5k.

**Largest size range taken.

AFDM, ash-free dry mass; tot, total; S.E.M., standard error of the mean. For other abbreviations, see text.

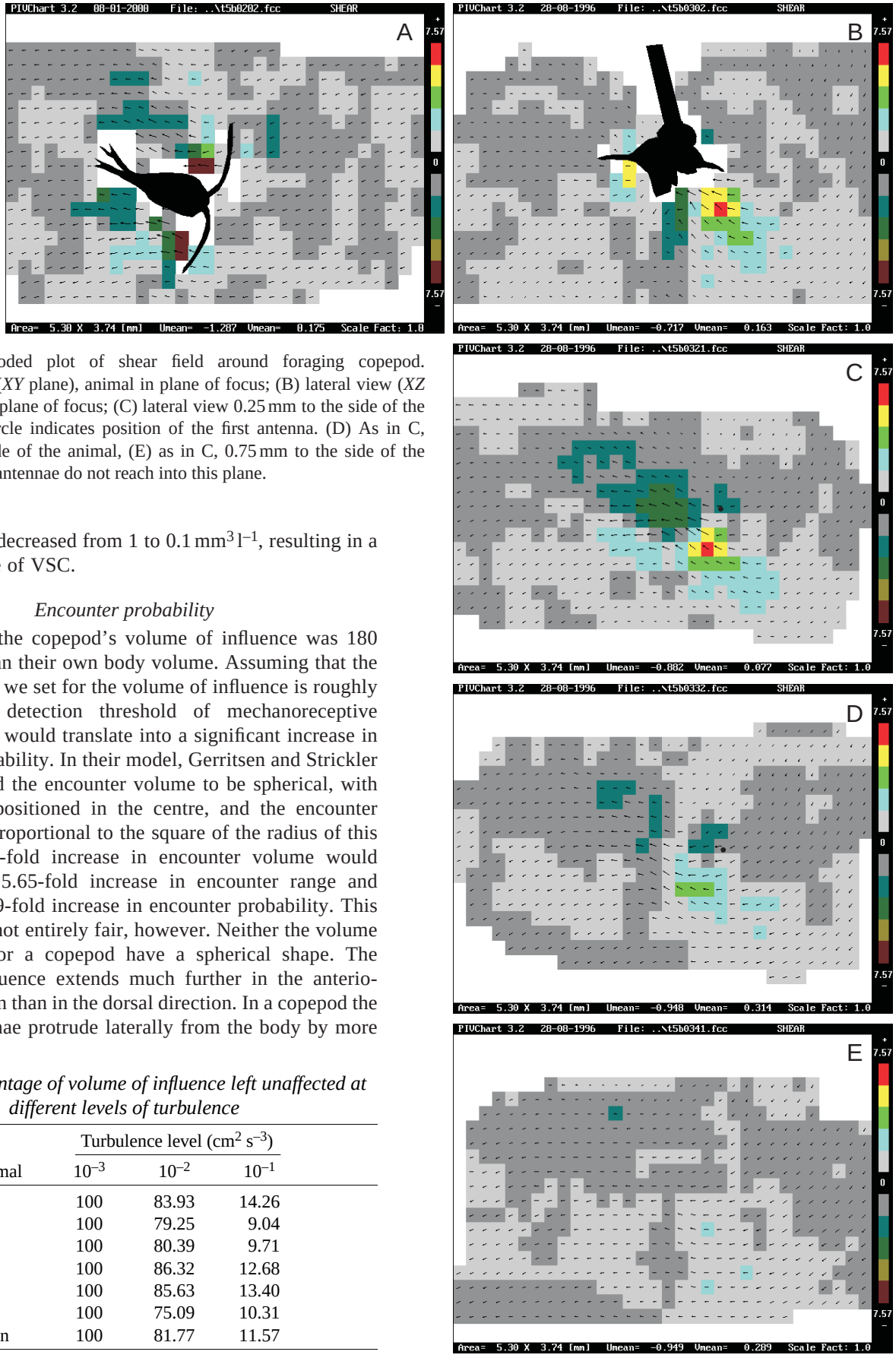

Fig. 6. Colour-coded plot of shear field around foraging copepod. (A) Dorsal view (*XY* plane), animal in plane of focus; (B) lateral view (*XZ* plane), animal in plane of focus; (C) lateral view 0.25 mm to the side of the animal. Black circle indicates position of the first antenna. (D) As in C, 0.5 mm to the side of the animal, (E) as in C, 0.75 mm to the side of the animal. The first antennae do not reach into this plane.

concentrations decreased from 1 to 0.1 $mm^3 l^{-1}$, resulting in a sixfold increase of VSC.

Encounter probability

On average the copepod's volume of influence was 180 times larger than their own body volume. Assuming that the threshold value we set for the volume of influence is roughly equal to the detection threshold of mechanoreceptive organisms, this would translate into a significant increase in encounter probability. In their model, Gerritsen and Strickler (1977) assumed the encounter volume to be spherical, with the organism positioned in the centre, and the encounter probability is proportional to the square of the radius of this sphere. A 180-fold increase in encounter volume would translate to a 5.65-fold increase in encounter range and therefore a 31.9-fold increase in encounter probability. This comparison is not entirely fair, however. Neither the volume of influence nor a copepod have a spherical shape. The volume of influence extends much further in the anterio-ventral direction than in the dorsal direction. In a copepod the two first antennae protrude laterally from the body by more

Table 4. *Percentage of volume of influence left unaffected at different levels of turbulence*

	Turbulence level ($cm^2 s^{-3}$)		
Animal	10^{-3}	10^{-2}	10^{-1}
T5a	100	83.93	14.26
T5b	100	79.25	9.04
T5d	100	80.39	9.71
T5f	100	86.32	12.68
T5k	100	85.63	13.40
T6l	100	75.09	10.31
Mean	100	81.77	11.57

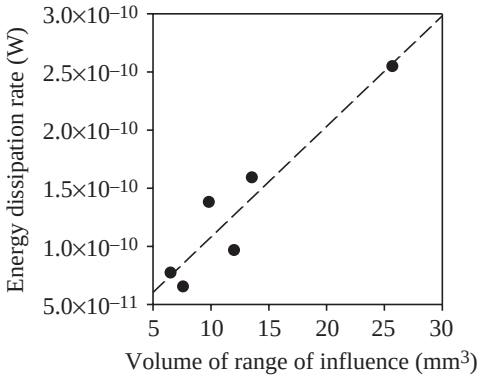

Fig. 7. Correlation between measured range of influence and rate of energy dissipation (r=0.94, P<0.05, N=6).

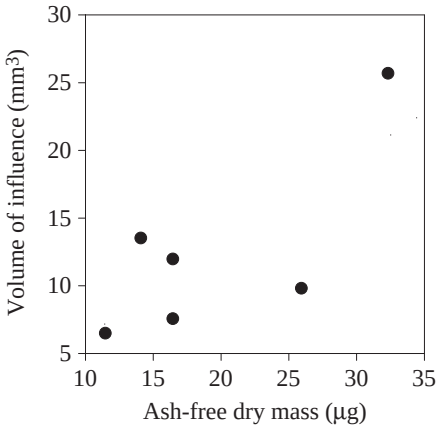

Fig. 8. Relation between volume of influence and body mass was not significant (r=0.76, P=0.08, N=6).

than 0.5 mm without contributing much to the body volume, and the same is true for the caudal rami. The effect of the feeding current on the encounter probability is therefore strongly dependent on the direction of approach of the other organism.

Effect of turbulence on feeding currents and feeding efficiency

The effect of turbulence on encounter probability has attracted a lot of attention (Marrasé et al., 1990; Costello et al., 1991; Kiørboe and Saiz, 1995; Saiz and Kiørboe, 1995). It is thought that turbulence may have a positive effect on encounter probability by increasing the average velocity of prey in the environment with respect to the predator. However, copepods with a very strong flow field probably benefit less from the effects of turbulence than copepods with a weak feeding current or those that follow a different feeding strategy altogether (Saiz and Kiørboe, 1995, Granata and Dickey, 1991). On the other hand, very high levels of turbulence could possibly erode the feeding current and thus have a negative effect on encounter probability (Saiz and Kiørboe, 1995).

Normal levels of turbulence in the upper mixed layer of the central North Sea range between 10^{-4} and 10^{-2} cm^2 s^{-3} (Saiz and Kiørboe, 1995; Granata and Dickey, 1991). From the data in Table 4 it is clear that only at levels of turbulence higher than normally experienced by *T. longicornis* would the rate of energy dissipation in the environment be higher than in most of the volume of influence. Even at the very high level of 0.1 cm^2 s^{-3}, nearly 12% of the volume of influence remains unaffected. The precise consequences of erosion of the volume in terms of reduced feeding and/or reduced perceptive abilities are quite difficult to assess, but these data indicate that under

Table 5. *Comparison of measured energy dissipation rate in feeding current to total energy consumption*

Species	Oxygen consumption	Power	Reference	Energetic cost of feeding current (% total) η_p=100%	Energetic cost of feeding current (% total) η_p=34%
Temora longicornis	0.0323 μl O_2 cop^{-1} h^{-1}	1.803×10^{-7} W cop^{-1}	Berner (1962)	0.293	0.861
Temora longicornis	0.0790 μl O_2 cop^{-1} h^{-1}	4.410×10^{-7} W cop^{-1}	Gauld and Raymont (1953)	0.120	0.352
Mesocyclops brasilianus	0.0153 μl O_2 cop^{-1} h^{-1}	8.565×10^{-8} W cop^{-1}	Epp and Lewis (1979)	0.617	1.813
Oithona similand	0.2200 μl O_2 cop^{-1} h^{-1}	5.118×10^{-8} W cop^{-1}	Nakamura and Turner (1997)	1.032	3.034
Centropages hamatus	0.06–0.12 μl O_2 cop^{-1} h^{-1}	3.35–6.70×10^{-7} W cop^{-1}	Zeuthen (1947)	0.07–0.15	0.231–0.463
Labidocera aestiva	2.5 μl O_2 mg DM^{-1} h^{-1}	1.396×10^{-5} W mg DM^{-1}	Vlymen (1970)	0.176*	0.517*
Acartia tonsa (1.2 mm)	35 nmol O_2 mg^{-1} h^{-1}	4.387×10^{-6} W mg AFDM^{-1}	Hoegh-Guldberg and Manahan (1995)	0.625	1.840
Mean ± S.E.M.				0.425±0.131	1.252±0.383

Cop, copepod; DM, dry mass; S.E.M., standard error of the mean.

Oxycaloric values: 1 ml O_2=20.1 J; 1 mg O_2=14.1 J.

Assumptions: η_m=25% (Goldspink, 1977; Morris et al., 1985); power (η_p=100%), 5.280×10^{-10} W cop^{-1}, 2.469×10^{-8} W mg DM^{-1}* or 2.744×10^{-8} W mg AFDM^{-1}; power (η_p=34%) 1.553×10^{-9} W cop^{-1}, 8.070×10^{-8} W mg DM^{-1}* or 7.263×10^{-8} W mg AFDM^{-1}.

*DM *T. longicornis* calculated assuming ash content of dry mass is similar to *T. stylifera*: 10.5% (Ivleva, 1980).

% total = energetic cost of the feeding current, calculated in this study, as a percentage of the total energy requirement, measured in the cited paper.

'normal' circumstances ambient turbulence will not have much negative effect on *T. longicornis*.

Energetic cost of the feeding current

When fish are swimming through water, or birds are flying through air, vortices containing kinetic energy are shed, while the animal propels itself forward (Spedding, 1986; Videler, 1993). Due to viscous friction these vortices will gradually dissipate and the kinetic energy will be converted into heat (Budó, 1980). Due to the low Reynolds number regime, foraging *T. longicornis* do not shed vortices. The energy that the animal puts into the water dissipates virtually immediately into heat, so the amount of viscous energy dissipation that we calculated should provide a reasonable estimate of the total rate of energy loss in the feeding current. This figure, however, does not represent the total cost of the feeding current to the animal. Losses will occur because the mechanical efficiency of the motion of the mouth parts (η_p) and the efficiency with which muscles transfer chemical energy into kinetic energy (η_m) will both be less than 1. Total swimming efficiency (η_{tot}) can be calculated as

$$\eta_{tot} = \eta_p \times \eta_m . \quad (9)$$

On the basis of their model, Morris et al. (1985) calculated a value for η_p of 34% for the pereopod swimming of *Pleuromamma xiphias*, during escape swimming. This low value for η_p is mainly due to the fact that escape swimming by pereopods results in a very jerky motion. High acceleration is reached during the power stroke of the pereopods, while the body decelerates during the recovery stroke. The standard swimming of *T. longicornis* is very smooth, and the resolution of our video system is not high enough to observe any pulsatility in the water motion due to the limb-beat frequency of copepods during standard swimming/foraging. It is of course unrealistic to assume that no acceleration and deceleration occurs, but it will by no means be as extreme as during pereopod swimming. Consequently, it is likely that η_p will be higher than calculated by Morris et al. (1985).

Assuming a mechanical efficiency of 100% as the ideal, and a muscle efficiency of 25% (Goldspink, 1977; Morris et al., 1985), the average power dissipating into the feeding current would result in an energetic cost of the feeding current of 5.28×10^{-10} W per animal or 2.74×10^{-5} W kg^{-1} AFDM (ash-free dry mass). Taking η_p to be 34%, as a worst case scenario, would result in a total cost of the feeding current of 1.55×10^{-9} W per animal or 7.26×10^{-5} W kg AFDM.

To assess whether the energetic cost of the feeding current represents an important part of the energy budget of *T. longicornis*, we need to compare the values of power necessary to generate a feeding current to the total energy requirements of this species. The most commonly used method to assess the energy requirements of organisms is to measure its rate of oxygen uptake. Table 5 lists a number of values of oxygen consumption measurements on copepods of similar size to *T. longicornis*, at temperatures between 15 and 20°C. The different oxygen consumption measurements show considerable variation. Gauld and Raymont (1953) measured a respiration rate in *T. longicornis* 2.4 times higher than Berner (1962) under similar circumstances. Despite this variation, and irrespective of the value chosen for the mechanical efficiency, our own estimates of the energetic cost of the feeding current for this copepod appear to represent only a small percentage of the total energy consumption of copepods in this size range.

We would like to thank Wim Klein Breteler for his help and advice with the copepod cultures and the regular supply of fresh stock, Anne van Kessel for her practical assistance with some of the pilot experiments, and Enric Saiz, Wim Wolff, Pete McLean and two anonymous referees for their useful comments on an earlier draft of this manuscript.

References

Alcaraz, M., Paffenhöfer, G. A. and Strickler, J. R. (1980). Catching the algae: A first account of visual observations on filter feeding calanoids. In *Evolution and Ecology of Zooplankton Communities. Special Symposium American Society of Limnology and Oceanography*, 57th edn (ed. W. C. Kerfoot), pp. 241-248. Hanover: University Press of New England.

Berner, A. (1962). Feeding and respiration in the copepod *Temora longicornis* (Müller). *J. Mar. Biol. Ass. UK* **42**, 625-640.

Budó, A. (1980). *Theoretische Mechanik*, Berlin: V.E.B. Deutscher Verlag der Wissenschaften.

Bundy, M. H. and Paffenhöfer, G. A. (1996). Analysis of flow fields associated with freely swimming calanoid copepods. *Mar. Ecol. Prog. Ser.* **133**, 99-113.

Costello, J. H., Strickler, J. R., Marrasé, C., Trager, G. and Zeller, R. (1991). Grazing in a turbulent environment: Behavioral response of a calanoid copepod, *Centropages hamatus*. *Proc. Natl. Acad. Sci. USA* **87**, 1648-1652.

Emlet, R. B. (1990). Flow fields around ciliated larvae: effects of natural and artificial tethers. *Mar. Ecol. Prog. Ser.* **63**, 211-225.

Epp, R. W. and Lewis, W. M. (1979). Metabolic responses to temperature change in a tropical freshwater copepod (*Mesocyclops brasilianus*) and their adaptive significance. *Oecologia* **42**, 123-138.

Fields, D. and Yen, J. (1993). Outer limits and inner structure: The 3-dimensional flow field of *Pleuromamma xiphias* (Calanoida: Metrinidae). *Bull. Mar. Sci.* **53**, 84-95.

Gauld, D. T. and Raymont, J. E. G. (1953). The respiration of some planktonic copepods II. The effect of temperature. *J. Mar. Biol. Ass. UK* **31**, 447-460.

Gerritsen, J. and Strickler, J. R. (1977). Encounter probabilities and community structure in zooplankton: a mathematical model. *J. Fish. Res. Board Can.* **34**, 73-82.

Gill, C. W. (1987). Recording the beat pattern of the second antennae of calanoid copepods. *Hydrobiologia* **148**, 73-78.

Goldspink, G. (1977). Muscle energetics and animal locomotion. In *Mechanics and Energetics of Animal Locomotion* (ed. R. McN. Alexander and G. Goldspink), pp. 57-81. London: Chapman and Hall

Granata, T. C. and Dickey, T. D. (1991). The fluid mechanics of copepods feeding in a turbulent flow: A theoretical approach. *Prog. Oceanog.* **26**, 243-261.

Hoegh-Guldberg, O. and Manahan, D. T. (1995). Coulometric measurement of oxygen consumption during developments of marine invertebrate embryos and larvae. *J. Exp. Biol.* **198**, 19-30.

Hwang, J. S., Turner, J. T., Costello, J. H., Coughlin, D. J. and Strickler, J. R. (1993). A cinematographic comparison of behavior by the calanoid copepod *Centropages hamatus* Lilljeborg: Tethered versus free-swimming animals. *J. Exp. Mar. Biol. Ecol.* **167**, 277-288.

Ivleva, I. V. (1980). The dependence of crustacean respiration rate on body mass and habitat temperature. *Int. Rev. Ges. Hydrobiol.* **65**, 1-47.

Kiørboe, T. and Saiz, E. (1995). Planktivorous feeding in calm and turbulent environments, with emphasis on copepods. *Mar. Ecol. Prog. Ser.* **122**, 135-145.

Klein Breteler, W. C. M., Fransz, H. G. and Gonzales, S. R. (1982). Growth and development of four calanoid copepod species under experimental and natural conditions. *Neth. J. Sea Res.* **16**, 195-207.

Klein Breteler, W. C. M. and Gonzales, S. R. (1986). Culture and development of *Temora longicornis* (Copepoda, Calanoida) at different conditions of temperature and food. *Syllogeus* **58**, 71-84.

Klyashtorin, L. B. and Yarzhombek, A. A. (1973). Energy consumption in active movements of planktonic organisms. *Oceanology* **13**, 575-580.

Lam, R. K. and Frost, B. W. (1976). Model of copepod filtering response to changes in size and concentration of food. *Limnol. Oceanogr.* **21**, 490-500.

Légier-Visser, M. F., Mitchell, J. G., Okubo, A. and Fuhrman, J. A. (1986). Mechanoreception in calanoid copepods: A mechanism for prey detection. *Mar. Biol.* **90**, 529-535.

Marrasé, C., Costello, J. H., Granata, T. and Strickler, J. R. (1990). Grazing in a turbulent environment: Energy dissipation, encounter rates, and efficacy of feeding currents in *Centropages hamatus*. *Proc. Natl. Acad. Sci. USA* **87**, 1653-1657.

Morris, M. J., Gust, G. and Torres, J. J. (1985). Propulsion efficiency and cost of transport for copepods: a hydromechanical model for crustacean swimming. *Mar. Biol.* **86**, 283-295.

Morris, M. J., Kohlhage, K. and Gust, G. (1990). Mechanics and energetics of swimming in the small copepod *Acanthocyclops robustus* (Cyclopoida). *Mar. Biol.* **107**, 83-91.

Nakamura, Y. and Turner, J. T. (1997). Predation and respiration by the small cyclopoid copepod *Oithona similis*: How important is feeding on ciliates and heterotrophic flagellates? *J. Plankton Res.* **19**, 1275-1288.

Paffenhöfer, G. A. and Harris, R. P. (1976). Feeding, growth and reproduction of the marine planktonic copepod *Pseudocalanus elongatus* Boeck. *J. Mar. Biol. Ass. UK* **56**, 327-344.

Paffenhöfer, G. A. and Lewis, K. D. (1990). Perceptive perfomance and feeding behaviour of calanoid copepods. *J. Plankton Res.* **12**, 933-946.

Poulet, S. A. and Gill, C. W. (1988). Spectral analyses of movements made by the cephalic appendages of copepods. *Mar. Ecol. Prog. Ser.* **43**, 259-267.

Saiz, E. and Kiørboe, T. (1995). Predatory and suspension feeding of the copepods *Acartia tonsa* in turbulent environments. *Mar. Ecol. Prog. Ser.* **122**, 147-158.

Schlichting, H. (1979). *Boundary Layer Theory*, 7th edn. New York: McGraw-Hill Inc.

Spedding, G. R. (1986). The wake of a jackdaw (*Corvus monedula*) in slow flight. *J. Exp. Biol.* **125**, 287-307.

Stamhuis, E. J. and Videler, J. J. (1995). Quantitative flow analysis around aquatic animals using laser sheet particle image velocimetry. *J. Exp. Biol.* **198**, 283-294.

Strickler, J. R. (1985). Feeding currents in calanoid copepods: two new hypotheses. In *Physiological Adaptations in Marine Animals* (ed. M. S. Laverack), pp. 459-485. Cambridge: Society for Experimental Biology.

Tiselius, P. and Jonsson, P. R. (1990). Foraging behaviour of six calanoid copepods: observations and hydrodynamic analysis. *Mar. Biol. Prog. Ser.* **66**, 23-33.

van Duren, L. A. and Videler, J. J. (1995). Swimming behaviour of developmental stages of the calanoid copepod *Temora longicornis* at different food concentrations. *Mar. Ecol. Prog. Ser.* **126**, 153-161.

Videler, J. J. (1993). *Fish Swimming*. London: Chapman and Hall.

Vlymen, W. J. (1970). Energy expenditure of swimming copepods. *Limnol. Oceanogr.* **15**, 348-356.

Yen, J. and Fields, D. M. (1992). Escape responses of *Acartia hudsonica* (copepoda) nauplii from the flow field of *Temora longicornis* (Copepoda). *Arch. Hydrobiol. Beih. Ergebn. Limnol.* **36**, 123-134.

Yen, J., Sanderson, B., Strickler, J. R. and Okubo, A. (1991). Feeding currents and energy dissipation by *Euchaeta rimana*, a subtropical pelagic copepod. *Limnol. Oceanogr.* **36**, 362-369.

Zeuthen, E. (1947). Body size and metabolic rate in the animal kingdom with special regard to marine micro-fauna. *Comp. Rend. Lab. Carlsberg, Ser. Chim. T* **26**, 17-161.